Curved nanowire structures and exciton binding energies

2009 J. Phys.: Condens. Matter 21 205302

(http://iopscience.iop.org/0953-8984/21/20/205302)

J. Phys.: Condens. Matter **21** (2009) 205302 (8pp) doi:10.1088/0953-8984/21/20/205302

Curved nanowire structures and exciton binding energies

M Willatzen and B Lassen

Mads Clausen Institute for Product Innovation, University of Southern Denmark, Alsion 2, DK-6400 Sønderborg, Denmark

E-mail: willatzen@mci.sdu.dk

Received 15 January 2009, in final form 13 March 2009
Published 24 April 2009
Online at stacks.iop.org/JPhysCM/21/205302

Abstract

Growth of quantum-confined semiconductor structures is a complicated process that may lead to imperfect and complex shapes as well as geometrical nonuniformities when comparing a large number of intended identical structures. On the other hand, the possibility of tuning the shape and size of nanostructures allows for extra optimization degrees when considering electronic and optical properties in various applications. This calls for a better understanding of size and shape effects. In the present work, we express the one-band Schrödinger equation in curved coordinates convenient for determining eigenstates of curved quantum-wire and quantum-dash structures with large aspect ratios. Firstly, we use this formulation to solve the problem of single-electron and single-hole states in curved nanowires. Secondly, exciton states for the curved quantum-wire Hamiltonian problem are found by expanding exciton eigenstates on a product of single-particle eigenstates. A simple result is found for the Coulomb matrix elements of an arbitrarily curved structure as long as the radius-of-curvature is much larger than the cross-sectional dimensions. We use this general result to compute the groundstate exciton binding energy of a bent nanowire as a function of the bending radius-of-curvature. It is demonstrated that the groundstate exciton binding energy increases by 40 meV as the radius-of-curvature changes from 20 to 2 nm while keeping the total length (and volume) of the nanowire constant.

(Some figures in this article are in colour only in the electronic version)

1. Introduction

Progress in semiconductor nanostructure growth has made it possible to design quantum-wire and quantum-dash structures of almost arbitrary shape and size [1–8]. It is well known experimentally and theoretically that spatial confinement strongly affects electronic and optical properties. Such confinement effects have led to considerable improvement in, for example, semiconductor lasers in terms of low threshold current, high modulation bandwidth, high differential gain, and small linewidth enhancement factor [9–11].

While size effects and implications for electronic eigenstates and associated energies are well understood, shape effects are not. This is mainly due to the fact that quasi-analytical parameter studies on more complex-shaped structures are scarce in the literature. In this paper, we employ a differential-geometry analysis so as to quasi-analytically obtain eigenstates and energies of arbitrarily curved nanowires subject to the condition that cross-sectional dimensions are small as compared to the quantum-wire length. Three ordinary differential equations in three curved coordinates u^1, u^2, u^3 are derived which can be easily solved either completely analytically in the three coordinates u^1, u^2, u^3 or analytically in two coordinates u^1, u^2 and quasi-analytically in the third coordinate u^3 [13, 14]. Next, we extend the analysis to consider the influence of excitonic couplings [15–18] in curved nanowires and obtain a simple Hamiltonian matrix problem formulation by expanding eigenstates of the full (excitonic) problem in eigenstates of the corresponding problem where excitonic effects are discarded.

It is demonstrated as a case study that for a nanowire of fixed total length and volume, constructed by interconnecting two straight sections via a 90° circular-bent section, the groundstate excitonic binding energy is strongly affected by the radius-of-curvature R of the circular section. In actual fact, the groundstate binding energy increases by around 40 meV as

R decreases from infinity (equivalent to a straight nanowire) to 2 nm.

2. The one-band effective-mass equation in a tubular neighborhood of a curve

In the first part of this section, we address electron and hole single-particle eigenstates corresponding to a curved quantum-wire structure in the framework of one-band $\vec{k}\cdot\vec{p}$ theory. Carriers are, for simplicity, assumed to be completely confined to the nanowire (infinite barriers). This assumption allows us to obtain simple results for eigenenergies, eigenstates and eventually excitonic binding energies even though in principle an analogous procedure can be carried out accounting for band-mixing effects and finite barriers, the latter corresponds to quantum dots embedded in a substrate/matrix material with a finite potential. Following the determination of single-particle energy states, we next analyze the excitonic Coulomb contribution to eigenstates by expanding the full Hamiltonian in terms of eigenstates for the Hamiltonian problem where Coulomb interactions are discarded. It is important to emphasize that the approach followed in this work does not require the exciton part of the Hamiltonian to be treated as a perturbation.

In the following, a detailed account of the theory behind conversion of the three-dimensional Schrödinger equation in Cartesian coordinates to appropriate curved coordinates (for which the problem reduces to the solution of three ordinary differential equations (ODEs)) is given along with the approximation of having small cross-sectional dimensions of the nanowire structure. Next, the analytical solutions to two of the ODEs are presented before providing three case studies for the third ODE.

2.1. Quantum-wire axis—arc-length parametrization

Consider a nanowire structure where the axis is given as a curve $\mathbf{r}(s)$ parametrized by arc length s. The tangent vector $\mathbf{t}(s) = \mathbf{r}'(s) = \mathrm{d}\mathbf{r}/\mathrm{d}s$ is a unit vector field along the curve and we can augment it with vector fields $\mathbf{p}(s)$ and $\mathbf{q}(s)$ along the curve such that $\mathbf{t}(s), \mathbf{p}(s), \mathbf{q}(s)$ constitutes an orthonormal frame at each point $\mathbf{r}(s)$ along the axis. Differentiation of the identities

$$\mathbf{t}\cdot\mathbf{t}=1, \qquad \mathbf{p}\cdot\mathbf{p}=1, \qquad \mathbf{q}\cdot\mathbf{q}=1,$$

$$\mathbf{t}\cdot\mathbf{p}=0, \qquad \mathbf{t}\cdot\mathbf{q}=0, \qquad \mathbf{p}\cdot\mathbf{q}=0,$$

yields

$$2\frac{\mathrm{d}\mathbf{t}}{\mathrm{d}s}\cdot\mathbf{t}=0, \qquad 2\frac{\mathrm{d}\mathbf{p}}{\mathrm{d}s}\cdot\mathbf{q}=0,$$

$$2\frac{\mathrm{d}\mathbf{p}}{\mathrm{d}s}\cdot\mathbf{q}=0, \qquad \frac{\mathrm{d}\mathbf{t}}{\mathrm{d}s}\cdot\mathbf{p}+\mathbf{t}\cdot\frac{\mathrm{d}\mathbf{p}}{\mathrm{d}s}=0,$$

$$\frac{\mathrm{d}\mathbf{t}}{\mathrm{d}s}\cdot\mathbf{q}+\mathbf{t}\cdot\frac{\mathrm{d}\mathbf{q}}{\mathrm{d}s}=0, \qquad \frac{\mathrm{d}\mathbf{p}}{\mathrm{d}s}\cdot\mathbf{q}+\mathbf{p}\cdot\frac{\mathrm{d}\mathbf{q}}{\mathrm{d}s}=0.$$

If we now let

$$a(s)=\frac{\mathrm{d}\mathbf{t}}{\mathrm{d}s}\cdot\mathbf{p}, \qquad b(s)=\frac{\mathrm{d}\mathbf{t}}{\mathrm{d}s}\cdot\mathbf{q}, \qquad c(s)=\frac{\mathrm{d}\mathbf{p}}{\mathrm{d}s}\cdot\mathbf{q},$$

then we obtain the following equation

$$\frac{\mathrm{d}}{\mathrm{d}s}\begin{bmatrix}\mathbf{t}\\ \mathbf{p}\\ \mathbf{q}\end{bmatrix}=\begin{bmatrix}0 & a & b\\ -a & 0 & c\\ -b & -c & 0\end{bmatrix}\begin{bmatrix}\mathbf{t}\\ \mathbf{p}\\ \mathbf{q}\end{bmatrix}. \tag{1}$$

Observe that the curvature κ of the axis is:

$$\kappa(s)=\left|\mathbf{r}''(s)\right|=\left|\mathbf{t}'(s)\right|=\sqrt{a^2+b^2}. \tag{2}$$

One way of obtaining vector fields $\mathbf{p}, \mathbf{q}$ is to let $\mathbf{p}$ be the principal normal $\mathbf{n}=\mathbf{t}'/\kappa$ and let $\mathbf{q}$ be the binormal $\mathbf{b}=\mathbf{t}\times\mathbf{n}$. In this case (1) becomes the Frenet–Serret equations [12], where $a=\kappa$, $b=0$ and $c=\tau$ the torsion of the axis.

We can now parametrize a tube around the axis, i.e. a tubular neighborhood in $\mathbb{R}^3$ of the curve $\mathbf{r}(s)$, according to:

$$\mathbf{x}(u^1,u^2,u^3)=\mathbf{r}(u^1)+u^2\mathbf{p}(u^1)+u^3\mathbf{q}(u^1). \tag{3}$$

The Laplace operator $\triangle_{\mathbb{R}^3}=\frac{\partial^2}{\partial x^2}+\frac{\partial^2}{\partial y^2}+\frac{\partial^2}{\partial z^2}$ in $\mathbb{R}^3$ is in curvilinear coordinates u^1, u^2, u^3 given by [13]

$$\triangle_{\mathbb{R}^3}=G^{ij}\partial_i\partial_j+\left(\frac{G^{ij}}{2}\frac{\partial_j G}{G}+\partial_j G^{ij}\right)\partial_i, \tag{4}$$

where $\partial_i=\frac{\partial}{\partial u^i}$, $[G_{ij}]^{-1}=[G^{ij}]$ and $G_{ij}=\frac{\partial\mathbf{x}_i}{\partial u^i}\cdot\frac{\partial\mathbf{x}_j}{\partial u^j}$ is the metric tensor. Neglecting operator contributions proportional to u^2 or u^3 in the Laplacian (assuming the quantum-wire cross-sectional dimensions to be much smaller than the quantum-wire length), we find [13]:

$$\begin{aligned}\triangle_{\mathbb{R}^3}&=G^{ij}\partial_i\partial_j+\left(G^{ij}\frac{\partial_j G}{2G}+\partial_j G^{ij}\right)\partial_i\\ &\approx \partial_1^2+\partial_2^2+\partial_3^2-a(u^1)\partial_2-b(u^1)\partial_3.\end{aligned} \tag{5}$$

Next, introduce

$$F=\sqrt{G}=1-u^2a(u^1)-u^3b(u^1), \tag{6}$$

and let $\chi=\sqrt{F}\psi$. Then we have, again to zeroth order in u^2, u^3,

$$\triangle_{\mathbb{R}^3}\psi\approx\partial_1^2\chi+\partial_2^2\chi+\partial_3^2\chi+\frac{\kappa^2}{4}\chi. \tag{7}$$

At this point it is important to emphasize that the result for the Laplace operator given by equation (7) shows that the solution to the Schrödinger equation χ can be separated in two parts f and g according to $\chi(u^1,u^2,u^3)=f(u^1)g(u^2,u^3)$ for *any* cross-sectional shape of the nanowire structure.

With the determination of the Laplace operator in curved coordinates $u^i (i=1,2,3)$, the Schrödinger equation for a quantum-mechanical particle of mass m and energy E reads (applies to zeroth order in u^1 and u^2):

$$\frac{-\hbar^2}{2m}\left(\partial_1^2\chi+\partial_2^2\chi+\partial_3^2\chi+\frac{\kappa^2}{4}\chi\right)+V(u^1,u^2,u^3)\chi=E\chi, \tag{8}$$

and the potential V satisfies:

$$V(u^1,u^2,u^3)=0, \tag{9}$$

if (u^1,u^2,u^3) is a point within the nanowire structure, i.e. the domain $-\epsilon^2\leqslant u^2\leqslant\epsilon^2$, and $-\epsilon^3\leqslant u^3\leqslant\epsilon^3$ in the

case of a nanowire having a rectangular-shaped cross-section. Similarly, the potential V is assumed infinite outside the nanowire structure.

As the curvature κ is a function of u^1 only it is immediately apparent that a separable solution $\chi = \chi_1(u^1)\chi_2(u^2)\chi_3(u^3)$ can be sought. Insertion into equation (8) gives

$$\partial_1^2\chi_1 + \left(\frac{\kappa^2}{4} - \lambda - \mu\right)\chi_1 = 0, \tag{10}$$

$$\partial_2^2\chi_2 + c^2\chi_2 = 0, \tag{11}$$

$$\partial_3^2\chi_3 + \left(\mu - c^2\right)\chi_3 = 0, \tag{12}$$

with $\lambda = -\frac{2mE}{\hbar^2}$ and c^3 and μ are separation constants. We also note the interesting fact that the form of the three ordinary differential equations (equations (10)–(12)) as well as associated boundary conditions (i.e. energies and eigenstates) are unchanged if the nanowire cross-section rotates with varying u^1 in the present approximation. This is so because varying the directions of the vectors $\mathbf{p}$ and $\mathbf{q}$ with u^1 does not influence the form of equations (10)–(12) or the boundary conditions.

2.2. Quantum-wire axis—general parametrization

In general, it is difficult to find an explicit arc-length parametrization $\mathbf{r}(s)$. Hence, we need to account for a general parametrization $\mathbf{r}(t)$ with $t = t(s)$ and $|\mathbf{r}'(t)| \neq 1$ as follows:

$$\frac{\mathrm{d}}{\mathrm{d}s} = \frac{\mathrm{d}t}{\mathrm{d}s}\frac{\mathrm{d}}{\mathrm{d}t} = \left(\frac{\mathrm{d}s}{\mathrm{d}t}\right)^{-1}\frac{\mathrm{d}}{\mathrm{d}t}, \tag{13}$$

$$\frac{\mathrm{d}\chi_1}{\mathrm{d}s} = \left(\frac{\mathrm{d}s}{\mathrm{d}t}\right)^{-1}\frac{\mathrm{d}\chi_1}{\mathrm{d}t}, \tag{14}$$

$$\begin{aligned}\frac{\mathrm{d}^2\chi_1}{\mathrm{d}s^2} &= \left(\frac{\mathrm{d}s}{\mathrm{d}t}\right)^{-1}\frac{\mathrm{d}}{\mathrm{d}t}\left(\left(\frac{\mathrm{d}s}{\mathrm{d}t}\right)^{-1}\frac{\mathrm{d}\chi_1}{\mathrm{d}t}\right)\\ &= \left(\frac{\mathrm{d}s}{\mathrm{d}t}\right)^{-2}\frac{\mathrm{d}^2\chi_1}{\mathrm{d}t^2} - \left(\frac{\mathrm{d}s}{\mathrm{d}t}\right)^{-3}\frac{\mathrm{d}^2s}{\mathrm{d}t^2}\frac{\mathrm{d}\chi_1}{\mathrm{d}t}.\end{aligned} \tag{15}$$

Now

$$\frac{\mathrm{d}s}{\mathrm{d}t} = |\mathbf{r}'(t)| = \sqrt{\mathbf{r}'\cdot\mathbf{r}'}, \tag{16}$$

$$\frac{\mathrm{d}^2s}{\mathrm{d}t^2} = \frac{\mathbf{r}'\cdot\mathbf{r}''}{\sqrt{\mathbf{r}'\cdot\mathbf{r}'}}, \tag{17}$$

$$\begin{aligned}\kappa^2 &= \frac{|\mathbf{r}'\times\mathbf{r}''|^2}{|\mathbf{r}'|^6} = \frac{(\mathbf{r}'\times\mathbf{r}'')\cdot(\mathbf{r}'\times\mathbf{r}'')}{(\mathbf{r}'\cdot\mathbf{r}')^3}\\ &= \frac{|\mathbf{r}'|^2|\mathbf{r}''|^2 - (\mathbf{r}'\cdot\mathbf{r}'')^2}{(\mathbf{r}'\cdot\mathbf{r}')^3}.\end{aligned} \tag{18}$$

In other words, in terms of an arbitrary parametrization of the curve, equation (10) becomes

$$\begin{aligned}\chi_1'' - \frac{\mathbf{r}'\cdot\mathbf{r}''}{\mathbf{r}'\cdot\mathbf{r}'}\chi_1' + \Bigg(&\frac{(\mathbf{r}'\cdot\mathbf{r}')(\mathbf{r}''\cdot\mathbf{r}'') - (\mathbf{r}'\cdot\mathbf{r}'')^2}{4(\mathbf{r}'\cdot\mathbf{r}')^2}\\ &- (\lambda+\mu)(\mathbf{r}'\cdot\mathbf{r}')\Bigg)\chi_1 = 0.\end{aligned} \tag{19}$$

2.3. Solutions to the χ_2 and χ_3 equations

The equations in χ_2 and χ_3 can be solved immediately. Firstly, the general solution to equation (11) in χ_2 is

$$\chi_2(u^2) = \sin\left(cu^2 + \phi_2\right), \tag{20}$$

where c and ϕ_2 are constants determined by the Dirichlet boundary conditions imposed, i.e.

$$\begin{aligned}\chi_2(-\epsilon^2) &= \sin\left(-c\epsilon^2 + \phi_2\right) = 0,\\ \chi_2(\epsilon^2) &= \sin\left(c\epsilon^2 + \phi_2\right) = 0.\end{aligned} \tag{21}$$

These conditions require

$$c = \frac{m'\pi}{2\epsilon^2}, \tag{22}$$

where m' is an integer different from zero. The other constant, the phase ϕ_2, is next chosen such that

$$\phi_2 = -c\epsilon^2, \tag{23}$$

and both Dirichlet conditions in equation (21) are now fulfilled. Apparently, when m' is even (and different from zero), χ_2 becomes

$$\chi_2(u^2) = \sin\left(\frac{m'\pi}{2\epsilon^2}u^2\right), \tag{24}$$

while for m' odd:

$$\chi_2(u^2) = \cos\left(\frac{m'\pi}{2\epsilon^2}u^2\right). \tag{25}$$

Similar arguments applied to equation (12) show that

$$\mu - c^2 = \left(\frac{n'\pi}{2\epsilon^3}\right)^2, \tag{26}$$

where n' is an integer different from zero. The eigenfunction χ_3 is (when n' is even (and different from zero))

$$\chi_3(u^3) = \sin\left(\frac{n'\pi}{2\epsilon^3}u^3\right), \tag{27}$$

while for n' odd:

$$\chi_3(u^3) = \cos\left(\frac{n'\pi}{2\epsilon^3}u^3\right). \tag{28}$$

Now, combining equations (22) and (26) allows μ to be specified

$$\mu = \left(\frac{m'\pi}{2\epsilon^2}\right)^2 + \left(\frac{n'\pi}{2\epsilon^3}\right)^2, \tag{29}$$

with $m' = \pm1, \pm2, \pm3$ and $n' = \pm1, \pm2, \pm3$. The possible values of the particle energy E are finally found from the χ_1 eigenvalue equation (equation (10)) by imposing appropriate boundary conditions given the value of μ (obtained from equation (29)).

3. Case studies

In order to show the application of the theory developed above, we consider three cases: a straight nanowire, a circular nanowire, and a helical nanowire. Parametrizations and curvature values as a function of the u^1 coordinate needed in deriving the χ_1 differential equation will be determined. We emphasize that a similar procedure can be carried out for an arbitrary parametrization using equation (19) instead of equation (10).

3.1. Straight quantum-wire axis

The straight quantum-wire parametrization is simply:

$$\mathbf{r}(u^1) = (u^1, 0, 0), \tag{30}$$

giving

$$|\mathbf{r}'(u^1)| = 1, \qquad |\mathbf{r}''(u^1)| = 0, \tag{31}$$

i.e. the parametrization is a parametrization by arc length. Hence, we may use the simpler equation (10) so as to determine χ_1.

Since $|\mathbf{r}''(u^1)| = 0$, the curvature is zero and equation (10) reads

$$\chi_1'' - (\lambda + \mu)\,\chi_1 = 0. \tag{32}$$

3.2. Circular quantum-wire axis

Consider next the circular-shaped quantum-wire axis with parametrization

$$\mathbf{r}(u^1) = \left(R\cos\left(\frac{u^1}{R}\right), R\sin\left(\frac{u^1}{R}\right), 0\right), \tag{33}$$

where R is the radius of the circle and

$$|\mathbf{r}'(u^1)| = 1, \qquad |\mathbf{r}''(u^1)| = \frac{1}{R}. \tag{34}$$

Since the circular-shaped quantum-wire axis of radius R is parametrized by arc length we may again use the simpler equation (10) to determine χ_1:

$$\chi_1'' - \left(\lambda + \mu - \frac{1}{4R^2}\right)\chi_1 = 0, . \tag{35}$$

3.3. Helical quantum-wire axis

A helical quantum-wire axis parametrization is:

$$\mathbf{r}(u^1) = \left(a\cos\left(\frac{u^1}{\sqrt{a^2+b^2}}\right), a\sin\left(\frac{u^1}{\sqrt{a^2+b^2}}\right), \frac{bu^1}{\sqrt{a^2+b^2}}\right), \tag{36}$$

where a is the radius and $2\pi b$ is the pitch length. Thus,

$$|\mathbf{r}'(u^1)| = 1, \qquad |\mathbf{r}''(u^1)| = \frac{a}{a^2+b^2}, \tag{37}$$

and an arc-length parametrization is obtained such that equation (10) applies:

$$\chi_1'' - \left(\lambda + \mu - \frac{a^2}{4\left(a^2+b^2\right)^2}\right)\chi_1 = 0. \tag{38}$$

The solution to the above equations is specified by the boundary conditions imposed. For a finite nanowire of length L with u^1 parameter range $0 < u^1 < L$, subject to an infinite-barrier potential outside the nanowire, the boundary conditions read:

$$\chi_1(u^1 = 0) = \chi_1(u^1 = L) = 0. \tag{39}$$

The above three cases are presented to demonstrate how easy the differential-geometry approach is to apply. In section 5, we combine the above wavefunction and energy eigenvalue results for the straight-line and circular quantum-wire axis cases to determine, in a simple way, exciton binding energies. We also point out that the circular region considered in section 5 could be replaced by a helix region or another curved region and addressed in a similar efficient way.

4. Computation of exciton binding energies

Let us proceed to determine a simple expression for the groundstate exciton binding energy assuming that electron and hole states both obey a one-band effective-mass equation. The one-band model equation for particles of mass m moving in a potential V is given by equation (8). In the preceding analysis, we have assumed that V only accounts for material confinement discarding the Coulomb interaction with other charged particles. Hence, the outputs of the above analysis are the single-particle envelope functions ϕ_{e}^k (electrons) and ϕ_{h}^l (holes) and the corresponding single-particle energies E_{e}^k (electrons) and E_{h}^l (holes).

For the exciton problem, the Coulomb interaction-energy contribution V_{cou} to the potential V reads:

$$V_{\mathrm{cou}} = \frac{1}{4\pi\epsilon}\frac{1}{|\vec{r}_{\mathrm{e}} - \vec{r}_{\mathrm{h}}|}, \tag{40}$$

where $\vec{r}_{\mathrm{e}}$, $\vec{r}_{\mathrm{h}}$ and ϵ denote the electron position vector, the hole position vector and the material permittivity, respectively.

We now compute the two-particle Coulomb matrix elements:

$$\begin{aligned} V_{\mathrm{cou}}^{klmn} &= \langle\phi_{\mathrm{e}}^m\phi_{\mathrm{h}}^n|V_{\mathrm{cou}}|\phi_{\mathrm{e}}^k\phi_{\mathrm{h}}^l\rangle \\ &= \int_V \mathrm{d}\vec{r}_{\mathrm{e}}\int_V \mathrm{d}\vec{r}_{\mathrm{h}}\,\phi_{\mathrm{e}}^{m*}(\vec{r}_{\mathrm{e}})\phi_{\mathrm{h}}^{n*}(\vec{r}_{\mathrm{h}})\frac{1}{4\pi\epsilon|\vec{r}_{\mathrm{e}} - \vec{r}_{\mathrm{h}}|} \\ &\quad\times \phi_{\mathrm{e}}^k(\vec{r}_{\mathrm{e}})\phi_{\mathrm{h}}^l(\vec{r}_{\mathrm{h}}). \end{aligned} \tag{41}$$

The two-particle Hamiltonian for non-interacting electrons and holes: H_0, acting on product states of single-particles, fulfils:

$$H_0|\phi_{\mathrm{e}}^k\phi_{\mathrm{h}}^l\rangle = E_0^{kl}|\phi_{\mathrm{e}}^k\phi_{\mathrm{h}}^l\rangle, \tag{42}$$

where E_0^{kl} is the pair energy of non-interacting electrons and holes in states k and l, respectively. Evidently, the pair energy is given by the sum of single-particle energies found by solving equation (10) as described above. We also have:

$$H = H_0 + V_{\mathrm{cou}}, \tag{43}$$

$$H|\psi_i\rangle = E_i|\psi_i\rangle, \tag{44}$$

where H, $|\psi_i\rangle$ and E_i are the total Hamiltonian including the Coulomb exciton interaction, the corresponding eigenstates and eigenenergies, respectively. Next, expanding $|\psi_i\rangle$ of the excitonic problem in pairs of single-particle states $|\phi_e^k\phi_h^l\rangle$:

$$|\psi_i\rangle = \sum_k \sum_l a_i^{kl} E_0^{kl} |\phi_e^k \phi_h^l\rangle, \tag{45}$$

with a_i^{kl} the expansion coefficients, we obtain:

$$\langle \phi_e^m \phi_h^n | H_0 | \psi_i \rangle = a_i^{mn} E_0^{mn}, \tag{46}$$

$$\langle \phi_e^m \phi_h^n | V_{cou} | \psi_i \rangle = \sum_k \sum_l a_i^{kl} V_{cou}^{klmn}. \tag{47}$$

Solutions $|\psi_i\rangle$ and E_i are now easily found by solving the secular equation:

$$||H - E_i|| = 0, \tag{48}$$

where $||\cdot||$ denotes the matrix determinant in a truncated set of coefficients a_i^{kl}. Generally speaking, for the (energetically) lower-lying states, usually only coefficients in a small set of (energetically) lower-lying pair states $|\phi_e^k\phi_h^l\rangle$ suffice to obtain an accurate solution.

The computation of exciton integrals V_{cou}^{klmn} is conveniently done by separating the integral in two parts: I_1^{klmn}, corresponding to $(*)$:$|\vec{r}_e - \vec{r}_h| \gg 2\epsilon_2, 2\epsilon_3$ and the rest $I_2^{klmn} = V_{cou}^{klmn} - I_1^{klmn}$. The criterion $(*)$ is satisfied for $z = u_e^1 - u_h^1$ if $|z| > \Delta$, where Δ is a numerical tuning parameter. In the computations, it was verified that V_{cou}^{klmn} is insensitive to the precise value of Δ as required. The two integrals I_1^{klmn} and I_2^{klmn} (apart from a prefactor $\frac{1}{4\pi\epsilon}$) now read:

$$\begin{aligned}
I_1^{klmn} &= \int_{-\Delta}^{\Delta} dz \int_0^L du_h^1\, F_1^{klmn}(z, u_h^1) \int_{-\epsilon_2}^{\epsilon_2} du_e^2 \int_{-\epsilon_2}^{\epsilon_2} du_h^2 \\
&\quad \times \int_{-\epsilon_3}^{\epsilon_3} du_e^3 \int_{-\epsilon_3}^{\epsilon_3} du_h^3\, F_2^{klmn}(u_e^2, u_h^2) F_3^{klmn}(u_e^3, u_h^3) \\
&\quad \times \frac{1}{\sqrt{\left(\vec{r}(z+u_h^1) - \vec{r}(u_h^1)\right)^2 + \left(u_e^2 - u_h^2\right)^2 + \left(u_e^3 - u_h^3\right)^2}}, \\
F_1^{klmn}(z, u_h^1) &= \chi_{e,1}^{m*}(z+u_h^1)\chi_{h,1}^{n*}(u_h^1)\chi_{e,1}^{k}(z+u_h^1)\chi_{h,1}^{l}(u_h^1), \\
F_2^{klmn}(u_e^2, u_h^2) &= \chi_{e,2}^{m*}(u_e^2)\chi_{h,2}^{n*}(u_h^2)\chi_{e,2}^{k}(u_e^2)\chi_{h,2}^{l}(u_h^2), \\
F_3^{klmn}(u_e^3, u_h^3) &= \chi_{e,3}^{m*}(u_e^3)\chi_{h,3}^{n*}(u_h^3)\chi_{e,3}^{k}(u_e^3)\chi_{h,3}^{l}(u_h^3),
\end{aligned} \tag{49}$$

$$\begin{aligned}
I_2^{klmn} &= \left(\int_{-L}^{-\Delta} dz + \int_{\Delta}^{L} dz\right) \\
&\quad \times \int_0^L du_h^1 \frac{F_1^{klmn}(z, u_h^1)}{|\vec{r}(z+u_h^1) - \vec{r}(u_h^1)|} \\
&\quad \times \int_{-\epsilon_2}^{\epsilon_2} du_e^2 \int_{-\epsilon_2}^{\epsilon_2} du_h^2 \int_{-\epsilon_3}^{\epsilon_3} du_e^3 \int_{-\epsilon_3}^{\epsilon_3} du_h^3 \\
&\quad \times F_2^{klmn}(u_e^2, u_h^2) F_3^{klmn}(u_e^3, u_h^3), \\
F_1^{klmn}(z, u_h^1) &= \chi_{e,1}^{m*}(z+u_h^1)\chi_{h,1}^{n*}(u_h^1)\chi_{e,1}^{k}(z+u_h^1)\chi_{h,1}^{l}(u_h^1), \\
F_2^{klmn}(u_e^2, u_h^2) &= \chi_{e,2}^{m*}(u_e^2)\chi_{h,2}^{n*}(u_h^2)\chi_{e,2}^{k}(u_e^2)\chi_{h,2}^{l}(u_h^2), \\
F_3^{klmn}(u_e^3, u_h^3) &= \chi_{e,3}^{m*}(u_e^3)\chi_{h,3}^{n*}(u_h^3)\chi_{e,3}^{k}(u_e^3)\chi_{h,3}^{l}(u_h^3),
\end{aligned} \tag{50}$$

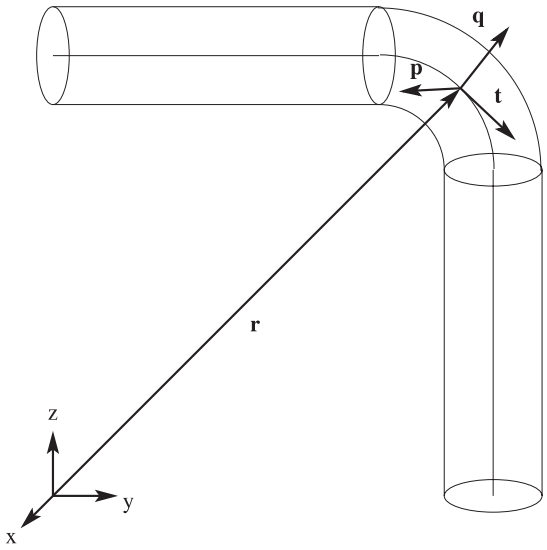

Figure 1. Schematics of the quantum-wire geometry considered as a case study in this work. The nanowire is composed of two straight sections interconnected by a 90° circular-bent section. For the test case considered, the total quantum-wire length is $L = 200$ nm and the quantum-wire diameter $2R$ is 2 nm.

In writing the expression for I_1^{klmn} we have used that $\mathbf{p}(u_h^1 + z) \approx \mathbf{p}(u_h^1)$ and $\mathbf{q}(u_h^1 + z) \approx \mathbf{q}(u_h^1)$ as the radius-of-curvature everywhere is much larger than Δ. Moreover, Δ is required to be much larger than the cross-sectional dimensions. Hence the restrictions in writing V_{cou}^{klmn} as $I_1^{klmn} + I_2^{klmn}$ are:

$$2\epsilon_2, 2\epsilon_3 \ll \Delta, \qquad \Delta \ll R(u^1), \tag{51}$$

where $0 \leqslant u^1 \leqslant L$. To simplify computations even more, we used an approximation for the denominator appearing in equation (49):

$$\begin{aligned}
&\frac{1}{\sqrt{(\vec{r}(z+u_h^1) - \vec{r}(u_h^1))^2 + (u_e^2 - u_h^2)^2 + (u_e^3 - u_h^3)^2}} \\
&= \frac{1}{\gamma\sqrt{\epsilon_2^2 + \epsilon_3^2 + |z|}},
\end{aligned} \tag{52}$$

where γ is a constant (it was verified numerically that $\gamma = 0.11$ gave good agreement). This procedure is similar to the one used in [19].

5. Numerical results and discussions

Consider the quantum-wire structure depicted in figure 1 composed of two straight sections interconnected by a circular-bent section. All three quantum-wire sections have the same cross-sectional geometry. We will choose the u^1 reference at the center of the nanowire, i.e.

$$\begin{aligned}
u^1 &\leqslant -\frac{\pi}{4}R; && \text{left straight section,} \\
-\frac{\pi}{4}R &\leqslant u^1 \leqslant \frac{\pi}{4}R; && \text{circular section,} \\
u^1 &\geqslant \frac{\pi}{4}R; && \text{right straight section.}
\end{aligned} \tag{53}$$

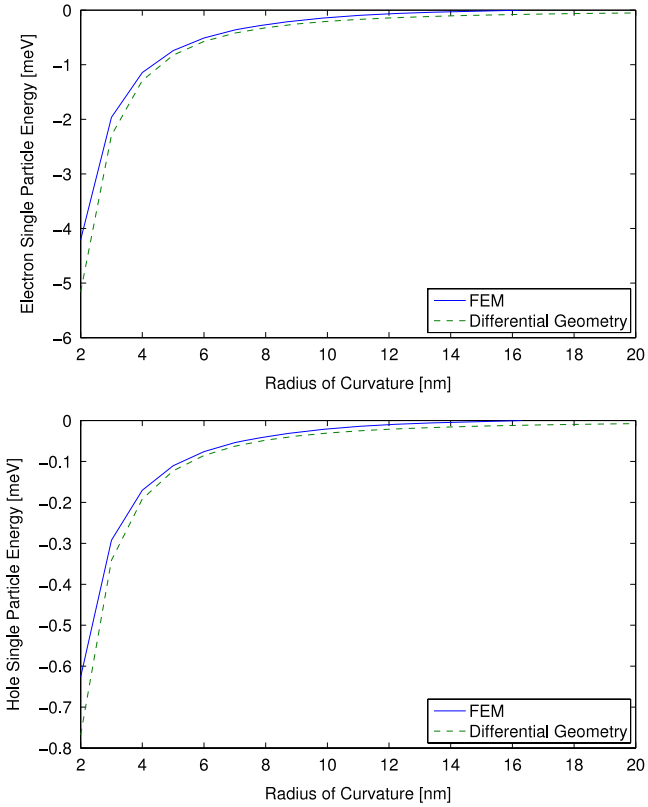

Figure 2. Plot of the single-particle electron energy (upper figure) and hole energy (lower figure) as a function of the radius-of-curvature for the quantum-wire structure shown in figure 1. The solid and dashed lines correspond to finite element and differential-geometry results, respectively. Energy contributions from confinement along the u^2 and u^3 directions are not included (refer to section 2.3 for the analytical expressions of these contributions). Units are meV and nm for energies and lengths, respectively.

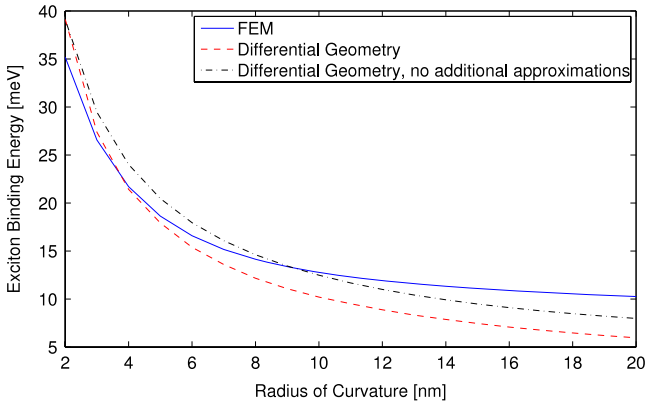

Figure 3. Plot of the exciton binding energy evaluated between single-particle electron and hole groundstates and the groundstate exciton binding energy as a function of the radius-of-curvature. The solid and dashed lines correspond to finite element and differential-geometry results, respectively. The dashed–dotted lines are differential-geometry results where no additional assumptions on the Coulomb element have been made, i.e. instead of using the approximate equations (49)–(52) we carry out the full six-dimensional integration. The quantum-wire structure considered is plotted in figure 1. The computed results are for $L = 200$ nm. Units are meV and nm for energies and lengths, respectively.

We assume, for simplicity, that electrons and holes obey a one-band effective-mass equation subject to infinite-barrier potentials outside the nanowire. This simplification allows us to emphasize the importance of curvature effects on eigenstates, eigenenergies, and excitonic binding energies instead of intermixing this with effects due to band mixing and incomplete confinement, effects that are well known and have been addressed to a large extent in the literature. We assume the nanowire to be made of GaAs with an electron effective mass of $0.067m_e$, heavy hole effective mass of $0.45m_e$, and a relative permittivity of 12.5 (m_e denotes the free electron mass) [20]. It is important to realize that the effective-mass approximation employed here is not reliable when quantum-wire diameters decrease below 2 nm, i.e. for wire radii below approximately 1 nm. In actual fact, inaccuracies of the $k \cdot p$ envelope function approximation results have been demonstrated in, for example, SnGe quantum-well superlattices when the individual layer thicknesses are a few number of lattice constants only (1–4 lattice constants) [21]. In the present work, since the radius-of-curvature is always higher than the quantum-wire radius, we do not expect additional limitations in using the EMA method due to the curvature of the quantum-wire. We emphasize that the quantum-wire diameter $2R$ used in the computations is 2 nm but the same trend in binding energy is found at higher radii. Experimentally, it is possible to fabricate GaAs quantum wires with such small diameters [8] and it is known that they are quite flexible. Hence, we choose in the following to compute energies down to a radius-of-curvature equal to 2 nm knowing well that the approximations in computing the Coulomb matrix elements (equations (49) and (50)) do not strictly apply down to 2 nm (we emphasize here that we also perform a full six-dimensional Coulomb-integral calculation where this approximation is not used).

Note also that we use for simplicity the bulk dielectric constant. However, it is important to stress that the effective dielectric constant of a nanostructure depends on the nanostructure geometry and material composition (refer to e.g. empirical pseudopotential and tight-binding calculations [22, 23]). Recently, a Thomas–Fermi model has been proposed [24] to obtain analytical results for the effective dielectric constant accounting for surface charge- and confinement effects of a semiconductor nanocrystal.

In figure 2, a plot of the groundstate electron (upper figure) and hole (lower figure) single-particle energies (discarding the Coulomb interaction) is plotted versus the radius-of-curvature R of the circular-bent section subject to a fixed total quantum-wire length L. Evidently, the groundstate energy (for electrons and holes) increases substantially with the decrease of the radius-of-curvature (note that the dependence is exactly as R^{-2}). We point out that this result is an analytical result using the fact that the straight- and circular-wire section problems can be solved and connected analytically (refer to sections 3.1 and 3.2 for the relevant ODEs).

In figure 3, the excitonic binding energy (lower figure), evaluated in the pair state formed between single-particle

groundstates of electrons and holes, is shown as a function of the radius-of-curvature of the circular-bent section. This matrix element is computed as the sum of integrals I_1^{1111} and I_2^{1111} using equations (49) and (50). Since all states but the single-particle groundstates are extended states (not exponentially decaying outside the circular section of the nanowire), $V_{\rm cou}^{klmn} \to 0$ as $L \to \infty$ whenever one of the indices k, l, m, n is different from 1. This fact guarantees that the groundstate exciton energy becomes:

$$E_{\rm ground}^{\rm exc} = E_{\rm e}^1 + E_{\rm h}^1 + V_{\rm cou}^{1111}, \tag{54}$$

as $L \to \infty$. Observe that the groundstate binding energy increases by approximately 40 meV as the radius-of-curvature decreases from 20 to 2 nm. The value of the binding energy due to quantum-wire bending is thus significant and will lead to important changes in, for example, photoluminescence spectra with varying degree of quantum-wire bending. In actual fact, the quantum-wire bending leads to spatial confinement of single-particle electron and hole groundstates at the bent section. This, in turn, leads to an enhanced groundstate exciton binding energy due to the small electron–hole distance (as a consequence of localized electron and hole groundstates) and the attractive Coulomb interaction.

5.1. Validation of the approach

For validation purposes, we have also carried out finite element method (FEM) calculations for the structure discussed in the previous section using the one-band model for electrons and holes but without any further approximations. As the FEM calculations can be carried out on finite domains only we have chosen to look at 200 nm long nanowires. The single-particle energies found using FEM are shown in figure 2 together with differential-geometry results. We observe that the differential-geometry and FEM approaches give very similar results, hence the former, due to its simplicity, is clearly useful for such structures.

We have also calculated the Coulomb element $V_{\rm cou}^{1111}$ without further approximations. In figure 3, we show the resulting binding energies as a function of the radius-of-curvature together with the binding energies found using the approach described in section 4. We again find good agreement between FEM results and differential-geometry results for small values of the radius-of-curvature. For larger radius-of-curvature values FEM calculations give higher binding energies. The higher binding energies are due to the finite length of the nanowire in the FEM calculations and are not a failure of the differential-geometry approach. Indeed, this has been checked by doubling the length of the nanowire and observing that the energies approach the differential-geometry results. The present work thus demonstrates that we not only capture single-particle energies with the simpler differential-geometry but also wavefunction related properties such as exciton binding energies.

We have also checked the approximations made in the Coulomb element calculations by directly evaluating the six-dimensional Coulomb integral using the wavefunctions found with the differential-geometry approach. The resulting binding energies as a function of the radius-of-curvature are shown as the dashed–dotted line in figure 3. Evidently, we capture the overall behavior using the proposed simplifications.

6. Benefits in using the differential-geometry approach

We point out that the differential-geometry approach presented allows for simplifications of the original three-dimensional Schrödinger equation for a complex-shaped nanowire structure to a single ordinary differential equation, in some cases allowing a completely analytical solution to be found. Furthermore, the use of the differential-geometry approach in combination with additional (numerically justified) assumptions reduces the original six-dimensional integral in the exciton binding energy calculation to a one-dimensional integral. This clearly highlights the potential of the present approach.

7. Conclusions

A simple method for determining the exciton binding energy of arbitrarily complex-shaped quantum-wire structures is presented by use of differential-geometry. The model allows us to express excitonic Coulomb matrix elements in curved coordinates which can be evaluated rather easily for a number of bent quantum-wire structures. As a case study, a nanowire composed of two straight sections interconnected by a 90° circular section is analyzed in detail. It is shown that the bending of the circular section leads to significant changes in the groundstate exciton binding energy of approximately 40 meV as the radius-of-curvature changes from 20 to 2 nm while keeping the total length and volume constant. Such changes will manifest themselves in photoluminescence spectra of curved quantum-wire structures.

References

[1] Masumoto Y and Takagahara T (ed) 2002 *Semiconductor Quantum Dots: Physics, Spectroscopy, and Applications* (New York: Springer)
[2] Prinz V Ya, Grützmacher D, Beyer A, David C, Ketterer B and Deckardt E 2001 *Nanotechnology* **12** 399–402
[3] Schmidt O G and Eberl K 2001 *Nature* **410** 168
[4] Matsutani S and Tsuru H 1991 *J. Phys. Soc. Japan* **60** 3640
[5] Tanda S, Tsuneta T, Okajima Y, Inagaki K, Yamaya K and Hatakenaka N 2002 *Nature* **417** 397
[6] Shimizu K T, Woo W K, Fisher B R, Eisler H J and Bawendi M G 2002 *Phys. Rev. Lett.* **89** 117401
[7] Duan X, Niu C, Sahi V, Chen J, Parce J W, Empedocles S and Goldman J L 2003 *Nature* **425** 274
[8] Duan X, Wang J and Lieber C M 2000 *Appl. Phys. Lett.* **79** 1116
[9] Arakawa Y and Sakaki H 1982 *Appl. Phys. Lett.* **40** 939
[10] Willatzen M, Tanaka T, Arakawa Y and Singh J 1994 *IEEE J. Quantum Electron.* **30** 640
[11] Willatzen M, Uskov A, Mørk J, Olesen H, Tromborg B and Jauho A-P 1991 *IEEE Photon. Technol. Lett.* **3** 606
[12] do Carmo M P 1976 *Differential Geometry of Curves and Surfaces* (Englewood Cliffs, NJ: Prentice-Hall)
[13] Gravesen J, Willatzen M and Lew Yan Voon L C 2005 *J. Math. Phys.* **46** 012107
[14] Gravesen J and Willatzen M 2005 *Phys. Rev.* A **72** 032108

[15] Kim S-S, Hong S-K and Yeon K-H 2007 *Phys. Rev.* B **76** 115322
[16] Fonoberov V A, Pokatilov E P and Balandin A A 2002 *Phys. Rev.* B **66** 085310
[17] Zhang C-J, Guo K-X and Lu Z-E 2007 *Physica* E **36** 92
[18] Bastard G 1988 *Wave Mechanics Applied to Semiconductor Heterostructures* (*Monographies de Physique*) (Les Ulis Cedex: Les Editions de Physique)
[19] Haug H and Koch S W 2004 *Quantum Theory of the Optical and Electronic Properties of Semiconductors* 4th edn (Singapore: World Scientific) p 125
[20] Hellwege H and Madelung O (ed) 1987 *Semiconductors, Intrinsic Properties of Group IV Elements and III–V, II–VI and I–VII Compounds* (*Landolt-Börnstein, New Series* Group III, vol 22 part a) (Springer: Berlin)
[21] Willatzen M, Lew Yan Voon L C, Santos P V, Cardona M, Munzar D and Christensen N E 1995 *Phys. Rev.* B **52** 5070
[22] Wang L W and Zunger A 1994 *Phys. Rev. Lett.* **73** 1039
[23] Lannoo M, Delerue C and Allan G 1995 *Phys. Rev. Lett.* **74** 3415
[24] Ninno D, Trani F, Cantele G, Hameeuw K J, Iadonisi G, Degoli E and Ossicini S 2006 *Europhys. Lett.* **74** 519